Wind Energ. Sci., 9, 49–64, 2024
https://doi.org/10.5194/wes-9-49-2024

eawe european academy of wind energy
Open Access WIND ENERGY SCIENCE

Nonlinear vibration characteristics of virtual mass systems for wind turbine blade fatigue testing

Aiguo Zhou[1], Jinlei Shi[1], Tao Dong[1], Yi Ma[1], and Zhenhui Weng[2]

[1]School of Mechanical Engineering, Tongji University, Shanghai 200082, China
[2]Aeolon Technology Co., Ltd, Shanghai 200120, China

Correspondence: Jinlei Shi (shijinlei1430@163.com)

Received: 31 July 2023 – Discussion started: 10 August 2023
Revised: 28 October 2023 – Accepted: 24 November 2023 – Published: 16 January 2024

Abstract. The biaxial fatigue test of wind turbine blades is helpful to shorten the test time and is more suitable for the actual operating conditions. Adding tuning masses to the blade is a common method for blade uniaxial testing at present, and its purpose is to adjust the load distribution in one direction of the blade. However, the tuning masses on the blade will affect the load distribution in the direction of the blade flap-wise and edge-wise at the same time in the biaxial test, so the concept of "virtual masses" is proposed to realize the decoupling of the load distribution in the biaxial test. Due to the limitation of the size of the virtual mass mechanism and the complex motion trajectory of the blade, the actual inertial effect provided by the virtual masses is different from the ideal situation, which will affect the resonance characteristics of the test system and the load distribution of the blade. Therefore, in order to evaluate the effect of the nonlinear effect introduced by the virtual masses on the resonance characteristics of the test system and the blade load distribution, the equivalent dynamic model of the bladed virtual mass test system was established by using the Lagrange method. Then, the nonlinear effects of blade amplitude and virtual mass installation parameters on the test system are obtained by a numerical method. Then, based on the nonlinear vibration theory, the approximate nonlinear amplitude–frequency characteristics of the test system are obtained, that is, the resonance frequency of the test system will decrease with the increase in the blade amplitude. Through the simulation analysis of two blades over 80 m in length, the applicability of the theoretical method is verified. It can be seen from the simulation results of the simulated uniaxial test that larger amplitudes of the blade and shorter connection rods will reduce the resonance frequency of the test system. When the vibration amplitude at the excitation point is the same, a lower resonance frequency results in a smaller load distribution level, that is, the area which is actually fully tested will be reduced. In the biaxial simulation test, the resonance frequency of the test system will be further reduced because the virtual masses will be affected by the coupled motion in both directions at the same time. Furthermore, the introduction of an external mechanism of the virtual mass will also cause deformation of the envelope of the blade biaxial trajectory, which will further affect the load distribution of the blade. This work explores the nonlinear influence of virtual masses on the actual fatigue test. The theoretical analysis is helpful to provide the basis and reference for the preliminary preparation work of the test organization, including adjusting the tuning mass scheme, adjusting the load distribution and selecting the appropriate excitation equipment.

Published by Copernicus Publications on behalf of the European Academy of Wind Energy e.V.

1 Introduction

As an important component of wind turbine, the cost of blades accounts for 20% of the overall machine, so the lifetime of blades is the premise to ensure safe and stable operation of the wind turbine (Zhang and Huang, 2015 ; Liao and Wu, 2016). To verify the reliability of the blade under the actual operating field, the International Electrotechnical Commission (IEC) points out that full-scale fatigue testing of rotor blades needs to be performed (IEC, 2014). In the actual blade fatigue test, two separate oscillation tests with over 1 million damage-equivalent loads cycles are usually performed.

The fatigue test requires that the load in the area of interest along the blade span-wise direction matches or exceeds the design value while keeping the exceedance as small as possible in order to avoid unrealistic failures (DNV GL AS, 2015). To satisfy the above requirements, additional masses are usually attached to the blade to tune the test load distribution, which needs to be optimized by determining the optimal mass distribution.

To save testing time and to emulate the comprehensive damage along the circumference of the blade, several institutions began to study and design biaxial fatigue tests (White, 2004; Greaves et al., 2012; Snowberg et al., 2014; Hughes et al., 1999; Liao and Wu, 2014), namely to excite the blade in both directions simultaneously. In the previous biaxial resonance test, a reasonable load distribution (in both directions) will be obtained by optimizing the position and tuning masses installed on the blade. However, the tuning masses installed on the blade will affect the vibration characteristics (mode shape and frequency) in both the flap-wise and edge-wise directions, which brings difficulty to the biaxial load match optimization, and there may be excessive overload in a certain area of the blade when choosing a compromise.

To simplify load match, the extra mechanism makes the tuning masses only act in one vibration direction (called virtual masses). The purpose of the virtual masses is to decouple the biaxial load so that the biaxial load match is equivalent to the combination of the load match of two single-axis tests. Post and Bürkner (2016) first proposed the concept of virtual masses to tune both natural frequencies independently in the two directions and to eliminate the coupling phenomenon of test bending moments during biaxial testing. Melcher et al. (2020a, b) used elastic elements to adjust blade stiffness and optimized biaxial fatigue test parameters based on virtual masses and elastic elements. Zhang et al. (2020) and Lu et al. (2022) carried out research on biaxial load matching and design using virtual masses. The virtual masses used for mass decoupling is ideally regarded as translational motion, and the push rod between the virtual mass and the blade is always in line with the main vibration in the above work, which is difficult to apply to the actual test field. A larger and stronger platform is needed to keep virtual mass translating in the edge-wise direction, which is difficult to achieve in a limited test space. In the biaxial test, the platform may interfere with the push rod, especially when the blade has a large amplitude in the flap-wise direction. Therefore, the Fraunhofer Institute for Wind Energy Systems (IWES) conducted further research; designed a device to convert virtual masses from translation to rotation; and applied it to the biaxial fatigue test, in which the frequency ratio of the two directions of the blade is adjusted to 1 : 1 by adjusting the virtual masses (Melcher et al., 2020c). Further, the feasibility of the biaxial decoupling test of the bending moment was verified by the comparison of simulation and experiment results (Melcher et al., 2020c; Castro et al., 2021; Falko, 2020). In fact, in view of the motion characteristics, the inertia force generated by rotating virtual masses is different from that generated by translational virtual masses. Taking a uniaxial test as an example, the translational virtual masses move synchronously with the blade, which behaves like a mass acting in just one direction from a numerical standpoint. The translational virtual masses have the same motion characteristics as the additional tuning masses. Therefore, although the virtual mass is not on the blade, the inertia force generated by it and the inertia force generated by the additional tuning masses are in the same direction and of the same magnitude. The rotating virtual masses are limited by the constraints of the seesaw, and their motion path is the rotating motion around the center of the seesaw. Therefore, the direction and magnitude of the inertial force generated by the rotation of the virtual mass will change, and it is not equivalent to the translational virtual masses. However, changes in the inertia force provided by the virtual masses will cause changes in the characteristics of the system, which may further cause changes in the blade load distribution and may put forward higher requirements for vibration excitation equipment.

To reveal the vibration mechanism of the blade-virtual-mass test system and provide a more rigorous theoretical basis for the biaxial load matching theory of the blade. In this paper, a theoretical model of the blade-virtual-mass uniaxial test system is established. The specific nonlinear impact of single parameters related to virtual masses on the characteristics of the test system can be obtained intuitively through the uniaxial model. Then, two blades over 80 m were simulated in ADAMS. Uniaxial simulation was used to verify the applicability of the theoretical model, including the nonlinear amplitude–frequency characteristics of the system and the effects of virtual mass installation parameters (such as seesaw length) on the load distribution of the blade. Biaxial simulation is used to analyze the nonlinear effect of virtual mass on the system under the simultaneous action of many factors. This work will be used in future research to adopt a reasonable control strategy and adjust the counterweight scheme in advance to achieve the target damage of the blade.

2 Blade-virtual-mass equivalent dynamic model

The tuning masses can change the modal characteristics of the testing system to adjust the test load distribution of the blade, which is essentially the bending moment caused by the inertia force brought by the reciprocating motion of the self-weight and tuning masses. In the common uniaxial fatigue test system, the tuning masses are directly attached to the blade, as shown in Fig. 1a. When the tuning masses are determined, the modal characteristics of the testing system are basically determined. This means that, without considering the air damping, the resonance frequency of the system remains unchanged.

In the biaxial fatigue test, the tuning masses decouple the biaxial load by seesaw, and the tuning masses are called virtual masses, as shown in Fig. 1b. The inertia force generated by the virtual masses mainly acts in the edge-wise direction in Fig. 1b. The mechanism for mounting the virtual masses consists of a push rod and a seesaw. The blade fixture, push rod and seesaw are connected through a universal joint, and the seesaw can rotate around the center position. Tuning masses are located at both ends of the seesaw to offset each other's gravity. After the exciting force is applied to the blade, the tuning masses move with the blade and rotate around the center of the seesaw to provide the inertia force for the blade through the push rod. However, due to the motion characteristics of the virtual mass mechanism, the motion of the virtual masses cannot be perfectly synchronized with the blade motion. Therefore, the inertia force generated by the rotation of the virtual masses differs from the inertia force generated by the traditional tuning masses. To evaluate the specific impact of a single parameter related to virtual masses on the test system, it is necessary to establish the corresponding uniaxial theoretical model for analysis from the perspective of the control variable method.

2.1 The comparison of the amplitude of inertia force

The uniaxial test is taken as an example to illustrate the difference between virtual mass translation and rotation, as shown in Fig. 2. The inertial force generated by rotating virtual masses of the blade at the maximum amplitude can be analyzed, as shown in Fig. 3. The relationship of the motion between virtual masses and the blade can be obtained:

$$\begin{cases} v_{\mathrm{m}} = v_{\mathrm{M}} + v_{\mathrm{mM}} \\ a_{\mathrm{m}} = a_{\mathrm{m}}^{\mathrm{n}} + a_{\mathrm{m}}^{\tau} = a_{\mathrm{M}} + a_{\mathrm{mM}}^{\mathrm{n}} + a_{\mathrm{mM}}^{\tau} \end{cases}, \tag{1}$$

where v_{m} is the velocity of virtual masses, v_{M} is the velocity of blade equivalent mass, v_{mM} is the relative velocity, $a_{\mathrm{mM}}^{\mathrm{n}}$ is the relative normal acceleration, a_{m} is the acceleration of the virtual masses, a_{mM}^{τ} is the relative tangential acceleration, $a_{\mathrm{m}}^{\mathrm{n}}$ is the normal acceleration, and a_{m}^{τ} is the tangential acceleration.

The blade at the maximum amplitude satisfies $v_{\mathrm{M}} = 0$, $v_{\mathrm{mM}} = 0$, $a_{\mathrm{mM}}^{\mathrm{n}} = 0$ and $a_{\mathrm{m}}^{\mathrm{n}} = 0$.

The angular acceleration of the virtual mass at the maximum amplitude of the blade can be obtained:

$$|\alpha_{\mathrm{m}}| = \frac{\omega^2 Y \cos(\beta_0)}{R\cos(\theta_0 - \beta_0)}, \tag{2}$$

where θ is the rotation angle of the seesaw at the maximum amplitude of the blade, β_0 is the angle between the push rod and the main vibration direction at the maximum amplitude of the blade, and α_{m} is the angular acceleration of the virtual mass at the maximum amplitude of the blade.

According to Eqs. (1) and (2), the rotating inertia force F_{R} generated by the rotating virtual mass at the maximum amplitude of the blade can be obtained:

$$F_{\mathrm{R}} = \frac{m\omega^2 Y \cos(\beta_0)}{\cos(\theta_0 - \beta_0)}. \tag{3}$$

The inertia force F_{rot} transmitted to the main vibration direction of the blade through the push rod can be obtained:

$$F_{\mathrm{rot}} = \frac{F_{\mathrm{R}}\cos(\beta_0)}{\cos(\theta_0 - \beta_0)} = \frac{m\omega^2 Y \cos^2(\beta_0)}{\cos^2(\theta_0 - \beta_0)}. \tag{4}$$

The translational virtual masses are consistent with the motion state of the blade, so the inertial force generated by the translational virtual masses can be obtained based on Eq. (4):

$$F_{\mathrm{tra}} = m\omega^2 Y. \tag{5}$$

According to Eqs. (4) and (5), there are differences in the inertial forces acting on the blades by the two setups, which are mainly caused by the difference in the movement trajectory of masses.

2.2 Model using the Lagrange method

In fact, there will be inertial force coupling in the actual biaxial testing process (virtual mass translation or rotation), which will cause multiple factors to work together and make it difficult to analyze the system characteristics quantitatively by a theoretical method. Therefore, it is desirable to choose the uniaxial test to analyze the nonlinear influence introduced by the virtual masses, which does not mean that the biaxial test can be regarded as the linear superposition of the uniaxial test. Essentially, the load distribution in the main vibration direction of the blade is adjusted by the component of the inertia force transmitted by the push rod in this direction. Because of the angle between the push rod direction and the vibration direction, blade displacement is not in line with the push rod. To more intuitively analyze the impact of virtual masses on the blade test system, the mass of the push rod and the seesaw are ignored in modeling according to the control variable method, and only their geometric dimensions are considered. Take the example of the blade edge-wise direction test; the blade model is simplified, as shown in Fig. 3. Moreover, the inertial force of the virtual masses also affects

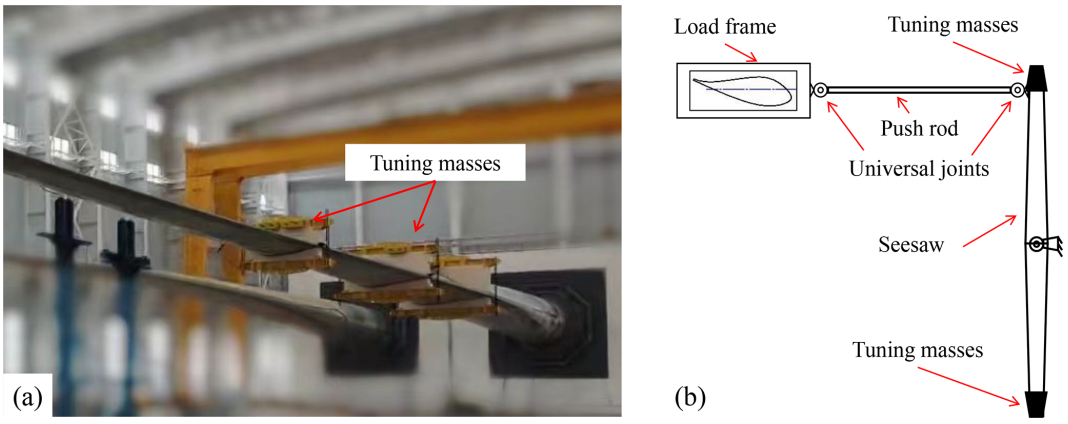

Figure 1. Mass match of blade fatigue test: **(a)** traditional tuning mass setup and **(b)** virtual mass setup.

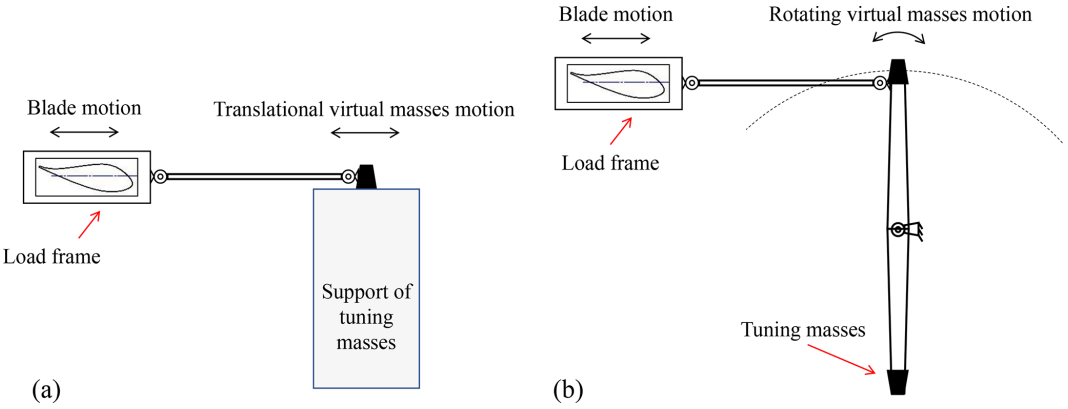

Figure 2. The comparison of inertia force: **(a)** translational-virtual-mass setup and **(b)** rotating-virtual-mass setup.

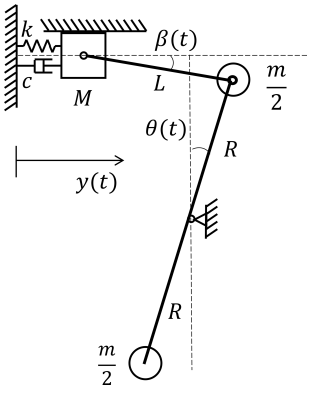

Figure 3. Virtual mass setup for blade fatigue test.

the flap-wise direction of the blade. However, since the frequency of the inertial force is close to the first-order modal frequency in the edge-wise direction, the perturbation to the flap-wise direction is relatively small. Therefore, only the influence of virtual masses on the vibration characteristics in the main testing direction needs to be considered during the uniaxial test. Section 2.1 only analyzes the difference in inertial force amplitude in Fig. 2, and this section set up a uniaxial theoretical model to evaluate the effect of virtual mass rotation on the vibration characteristics of the test system. In this paper, the Lagrange method is used to analyze the uniaxial model (Liu et al., 2019). The initial state of the test system is assumed when the blade is stationary, the push rod is horizontal, and the seesaw is vertical.

$$\frac{\mathrm{d}}{\mathrm{d}t}\left(\frac{\partial T}{\partial \dot{q}_j}\right) - \frac{\partial T}{\partial q_j} + \frac{\partial V}{\partial q_j} + \frac{\partial D}{\partial \dot{q}_j} = Q_j \, j = 1, 2, \ldots, n, \quad (6)$$

where T is the kinetic energy, V is the potential energy, D is the dissipated energy, q_j is the generalized coordinate, $\dot{q}_j$ is the generalized velocity, and Q_j is the generalized force.

By selecting the generalized coordinate $q = y$, and based on the motion relationship in Fig. 3, the displacement and velocity relationships of the test system can be obtained:

$$\begin{cases} y + L\cos\beta - R\sin\theta = L \\ L\sin\beta + R\cos\theta = R \end{cases} \quad (7)$$

$$\begin{cases} \dot{y} - L\dot{\beta}\sin\beta - R\dot{\theta}\cos\theta = 0 \\ L\dot{\beta}\cos\beta - R\theta\sin\theta = 0 \end{cases}. \tag{8}$$

T, V and D can be calculated as

$$T = \frac{1}{2}M\dot{y}^2 + \frac{1}{2}mR^2\dot{\theta}^2 = \frac{1}{2}M\dot{y}^2 + \frac{1}{2}m\dot{y}^2\frac{\cos^2\beta}{\cos^2(\theta-\beta)} \tag{9}$$

$$V = \frac{1}{2}ky^2 \tag{10}$$

$$D = \frac{1}{2}c\dot{y}^2, \tag{11}$$

where L is the length of the push rod, R is the radius of the seesaw, β is the angle between the push rod and the horizontal direction, θ is the angle between the seesaw and the vertical direction, M is the blade equivalent mass, m is the virtual masses, k is the blade equivalent stiffness, and c is the blade equivalent damping.

According to Eqs. (7) and (8), the relevant terms in Eq. (6) are obtained as

$$\begin{cases} \frac{\mathrm{d}}{\mathrm{d}t}\left(\frac{\partial T}{\partial \dot{y}}\right) = M\ddot{y} + m\ddot{y}\frac{\cos^2\beta}{\cos^2(\theta-\beta)} + m\dot{y}\frac{\mathrm{d}}{\mathrm{d}t}\left[\frac{\cos^2\beta}{\cos^2(\theta-\beta)}\right] \\ \frac{\partial T}{\partial y} = \frac{1}{2}m\dot{y}^2\frac{\partial}{\partial y}\left[\frac{\cos^2\beta}{\cos^2(\theta-\beta)}\right] \\ \frac{\partial V}{\partial y} = ky \\ \frac{\partial \Psi}{\partial \dot{y}} = c\dot{y} \\ Q(t) = F(t) \end{cases}. \tag{12}$$

Then, the dynamic differential equation of the test system is obtained as

$$\left\{M + m\frac{\cos^2\beta}{\cos^2(\theta-\beta)}\right\}\ddot{y} + c\dot{y} + ky + \frac{m\dot{y}^2\cos\beta}{\cos^4(\theta-\beta)}\left[\frac{\cos^2\beta\sin(\theta-\beta)}{R} - \frac{\sin^2\theta}{L}\right] = F(t). \tag{13}$$

By comparison with Eq. (4), it can be seen that the inertial force terms of two equations are the same at the maximum amplitude of the blade, where

$$\sin\theta = \frac{L+y}{R} - \frac{L\left(R\sqrt{-\left(y^2+2Ly-2LR\right)\left(y^2+2Ly+2LR\right)} + y^3 + 2L^3 + 4L^2y + 3Ly^2\right)}{2R\left(L^3+2L^2y+LR^2+Ly^2\right)}$$

$$\cos\theta = \frac{L(L+y)\left[R\sqrt{-\left(y^2+2Ly-2LR\right)\left(y^2+2Ly+2LR\right)} + 2L^3 + y^3 + 3Ly^2 + 4L^2y\right]}{2R^2\left(L^3+2L^2y+LR^2+Ly^2\right)} - \frac{2L^2+2Ly-2R^2+y^2}{2R^2}$$

$$\sin\beta = \frac{2L^2+2Ly+y^2}{2LR} - \frac{(L+y)\left[R\sqrt{-\left(y^2+2Ly-2LR\right)\left(y^2+2Ly+2LR\right)} + 2L^3 + y^3 + 3Ly^2 + 4L^2y\right]}{2R\left(L^3+2L^2y+LR^2+Ly^2\right)}$$

$$\cos\beta = \frac{R\sqrt{-\left(y^2+2Ly-2LR\right)\left(y^2+2Ly+2LR\right)} + 2L^3 + y^3 + 3Ly^2 + 4L^2y}{2\left(L^3+2L^2y+LR^2+Ly^2\right)}.$$

According to Eq. (13), it can be seen that rotation of virtual masses introduces nonlinear terms to the test system, and both the angle θ and β are nonlinear functions of the blade response y. Due to the complexity of the dynamic equation, it is difficult to obtain the corresponding analytical expression. Therefore, the numerical analysis methods are used to solve the equation. A numerical simulation model based on the differential equation of the system motion is established in MATLAB SIMULINK, and the corresponding resonance frequency of the equivalent system can be obtained by setting different initial displacements. By modifying the value of the different parameter, the influence of the parameter change on the resonance frequency of the test system can be obtained. As mentioned previously, the nonlinear factors that affect the characteristics of the test system mainly come from installation parameters (push rod length and seesaw radius) and blade response. The design length of the push rod generally remains unchanged due to space limitations at the test site. However, the seesaw radius offers greater design flexibility. Thus, the primary focus is on evaluating the impact of the seesaw radius R and blade response y on the vibration characteristics of the blade. To illustrate this, the equivalent parameters of the 80 m blade are brought into the differential equation and numerically analyzed, and the influence of the blade amplitude on the resonance frequency of the test system is investigated, as demonstrated in Fig. 4.

Figure 4a shows that the resonance frequency of the test system decreases nonlinearly with an increase in blade amplitude, and virtual mass m further determines the rate of decrease in resonance frequency. The equivalent stiffness k has the ability to alter the natural frequency of the test system. However, it can be seen from Fig. 4b that k cannot change the rate of decrease in resonance frequency with other parameters unchanged, which indicates that the equivalent stiffness is not a nonlinear factor affecting the vibration characteristics of the testing system. Figure 4c shows that the increase in M will delay the decline rate of the natural frequency of the system because the proportion of the virtual masses in the inertia force term decreases. It can be seen from Fig. 4d that the radius of the seesaw will also affect the nonlinear amplitude–frequency characteristics of the test system and the rate of decrease in resonance frequency.

2.3 Analysis of amplitude–frequency characteristics of the model

The dynamic differential equations of the blade-virtual-mass test system, established through the Lagrange method, are highly complex and can only be resolved numerically to derive the correlations among the relevant parameters and the resonance frequency of the test system. To further analyze the nonlinear amplitude–frequency characteristics of the test system, it is necessary to create a theoretical model of the test system based on nonlinear dynamics (Liu and Chen, 2001). According to linear vibration theory (Liu et al., 2019), the

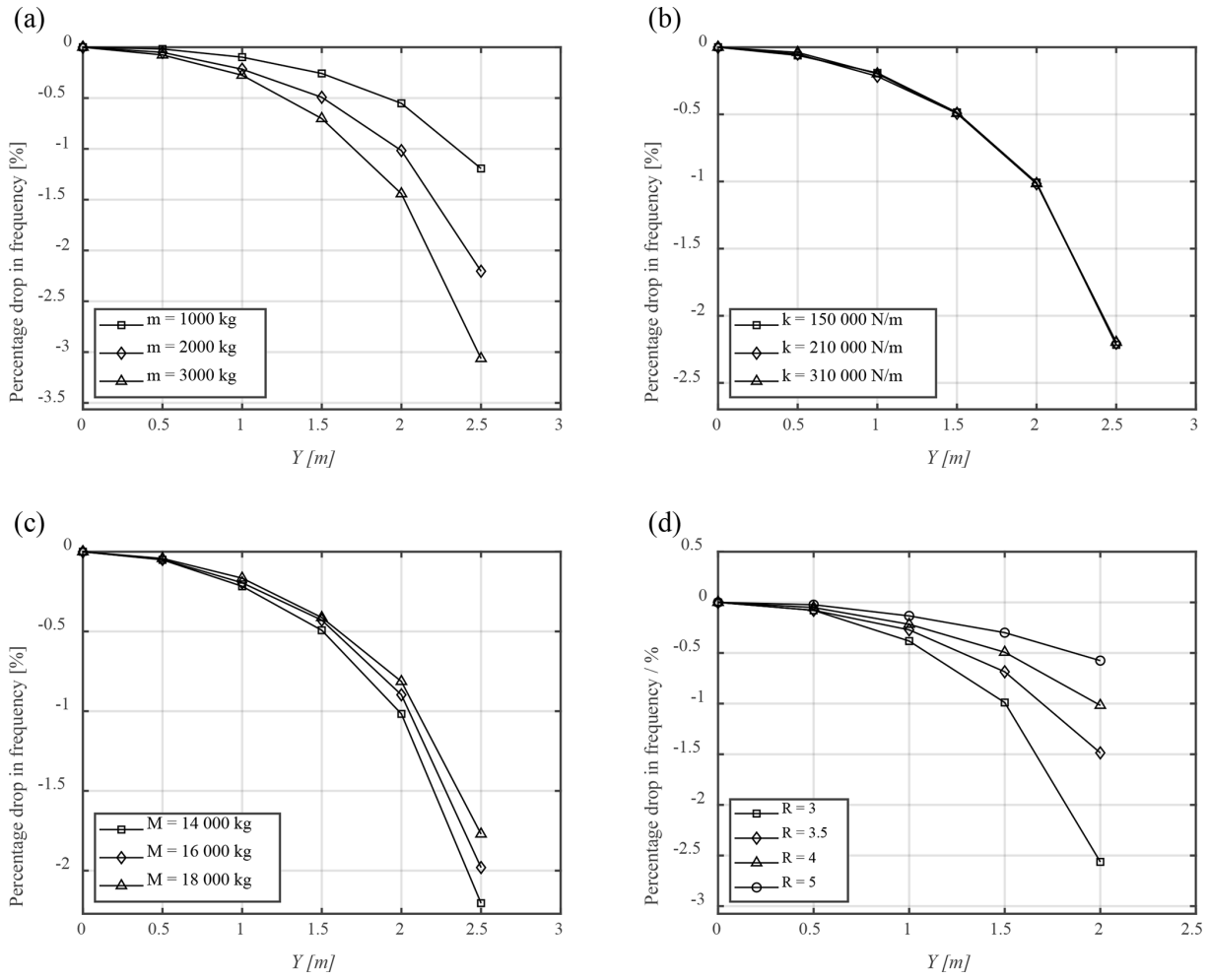

Figure 4. The relationship between resonance frequency and amplitude of the blade with different parameters: **(a)** $M = 14000\,\mathrm{kg}$, $k = 210000\,\mathrm{N\,m^{-1}}$, $L = 4\,\mathrm{m}$, $R = 4\,\mathrm{m}$; **(b)** $M = 14000\,\mathrm{kg}$, $m = 2000\,\mathrm{kg}$, $L = 4\,\mathrm{m}$, $R = 4\,\mathrm{m}$; **(c)** $k = 210000\,\mathrm{N\,m^{-1}}$, $m = 2000\,\mathrm{kg}$, $L = 4\,\mathrm{m}$, $R = 4\,\mathrm{m}$; **(d)** $M = 14000\,\mathrm{kg}$, $k = 210000\,\mathrm{N\,m^{-1}}$, $m = 2000\,\mathrm{kg}$, $L = 4\,\mathrm{m}$.

factors that primarily influence the inherent characteristics of a linear system are the inertial force term and the elastic force term. In fact, the inherent characteristics of the blade-virtual-mass test system are primarily determined by the inertial force term associated with the introduction of virtual masses and the response of the blade. Thus, the weakly nonlinear dynamic equation of the blade-virtual-mass test system in Eq. (13) can be approximated as

$$(M+m)f(y)\ddot{y} + c\dot{y} + ky = F_0\cos(\omega t + \theta), \tag{14}$$

where $f(y) = 1 + \varepsilon_1 y + \varepsilon_2 y^2 + \varepsilon_3 y^3 + \varepsilon_4 y^4$; $c = 2\zeta(M+m)\omega_n$; $k = (M+m)\omega_n^2$; $F_0 = Bk$; ε_1, ε_2, ε_3 and ε_4 are small parameters related to M, m, L and R; ζ is the damping ratio; ω_n is the natural frequency; ω is the excitation frequency; and θ is the phase difference between steady-state response and excitation.

Ignoring the small parameters, Eq. (14) is transformed into the vibration equation of a linear system. This means that the linear system is derived from the original nonlinear system. To quantitatively analyze the modal characteristics of the test system, the approximate analytical method can be employed by considering the nonlinear factor as a perturbation to the linear system, yielding an approximate analytical solution for the nonlinear system. Among various approximate analytical methods, the harmonic balance method is particularly notable due to its clear conceptual foundation. It expands both the excitation term and the solution of the equation into a Fourier series. From a physical perspective, the coefficients of the harmonic terms of the same order at both ends of the dynamic equation must be equal to maintain a balance between the excitation and inertia forces. When the condition of the test system is determined, the value of the small parameter in Eq. (14) is also determined.

For the blade-virtual-mass test system, it is assumed that its steady-state response is still periodic, but the resonance frequency is different from the natural frequency of the de-

rived system. The basic solution is expanded into the Fourier series of the excitation frequency, and the fundamental component is retained. The response of the system is indicated by Eq. (15).

$$y(t) = Y_0 \cos(\omega t), \tag{15}$$

where Y_0 is the amplitude of the blade steady-state response.

By substituting Eq. (15) into Eq. (14) and applying the triangle transform and harmonic balance to eliminate the phase difference θ, the relationship between the amplitude and frequency of the test system is indicated by Eq. (16).

$$\left[1 - s^2\left(1 + \frac{3}{4}\varepsilon_2 Y_0^2 + \frac{10}{16}\varepsilon_4 Y_0^4\right)\right]^2 + (2\zeta s)^2 = \left(\frac{B}{Y_0}\right)^2, \tag{16}$$

where $s = \omega/\omega_n$.

According to Eq. (16), the amplitude–frequency and phase–frequency characteristics of the nonlinear system can be obtained, as Eq. (17) indicates.

$$\begin{cases} \frac{Y_0}{B} = \frac{1}{\sqrt{\left[1-s^2\left(1+\frac{3}{4}\varepsilon_2 Y_0^2+\frac{10}{16}\varepsilon_4 Y_0^4\right)\right]^2+(2\zeta s)^2}} \\ \theta = \arctan\left[\frac{2\zeta s}{1-s^2\left(1+\frac{3}{4}\varepsilon_2 Y_0^2+\frac{10}{16}\varepsilon_4 Y_0^4\right)}\right] \end{cases} \tag{17}$$

When $\varepsilon_2 = \varepsilon_4 = 0$, Eq. (17) describes the amplitude–frequency characteristics of a linear system, as shown in Fig. 5. When the small parameters are non-zero, the amplitude–frequency characteristic curve of the nonlinear system is depicted in Fig. 6. Similar to forced vibrations in linear systems, nonlinear systems also exhibit similar amplitude–frequency characteristic curves. However, the backbone of the support curve clusters is not straight but inclined. This backbone curve represents the variation in the free-vibration frequency of the nonlinear system with respect to the amplitude when there is no external excitation (Liu and Chen, 2001). By setting $B = 0.1$ and $\zeta = 0$ in Eq. (16), the equation for this backbone curve can be obtained, as Eq. (18) indicates.

$$\omega^2 = \frac{\omega_n^2}{\left(1 + \frac{3}{4}\varepsilon_2 Y_0^2 + \frac{10}{16}\varepsilon_4 Y_0^4\right)} \tag{18}$$

Equation (18) shows that the resonance frequency of the blade-virtual-mass test system decreases with an increase in the amplitude of the blade, and there exists the nonlinear relationship between the square of the frequency ratio and the amplitude. Figure 6 shows that the small parameters in the inertial force term will affect the frequency of free vibration. As these small parameters decrease, the amplitude–frequency characteristic curve of a nonlinear system approaches that of a linear system, and the backbone curve approaches a value close to 1.

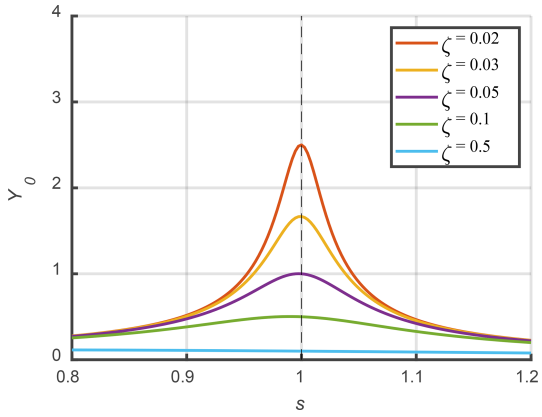

Figure 5. Amplitude–frequency characteristic curve of a linear system.

Figure 6 shows the influence of different small parameters on the amplitude–frequency characteristics of the system. In fact, specific small parameter values mean specific working conditions, that is, when the virtual-mass-related parameters (such as L, R and m) are determined, the amplitude–frequency characteristics of the system will also be determined. Therefore, as long as the setups are determined, the dynamic characteristics of the test system will be determined, whether it is a uniaxial axis test or a biaxial test.

In addition, the amplitude hopping phenomenon, also known as dynamic bifurcation, also appears in Fig. 6. In fact, there is no obvious dynamic bifurcation phenomenon in the fatigue test because the nonlinearity of the system is weak, and the amplitude of the blade is limited by the size of the mechanism. Moreover, when the influence of blade amplitude on the resonance frequency of the system is discussed in the following part of this paper, more attention is paid to the backbone curve in the shape of the dotted black line in Fig. 6.

3 Dynamic simulation analysis

To validate the nonlinear characteristics of the blade-virtual-mass test system that has been established, it is necessary to utilize the multi-body dynamic simulation software ADAMS to create a realistic blade model for analysis. Based on the sectional properties and tuning masses of the blade, ADAMS can be employed for modeling and analyzing the blade-virtual-mass system. ADAMS can perform modal analysis and transient sweep-frequency analysis to obtain the changing characteristics of the test system under various operating conditions. As the foundation for other dynamic analysis, modal analysis is used to determine the modal characteristics of structures. Regarding the weakness of modal analysis function in the software, which cannot consider the effects of the response on the modal characteristics of the system, it is

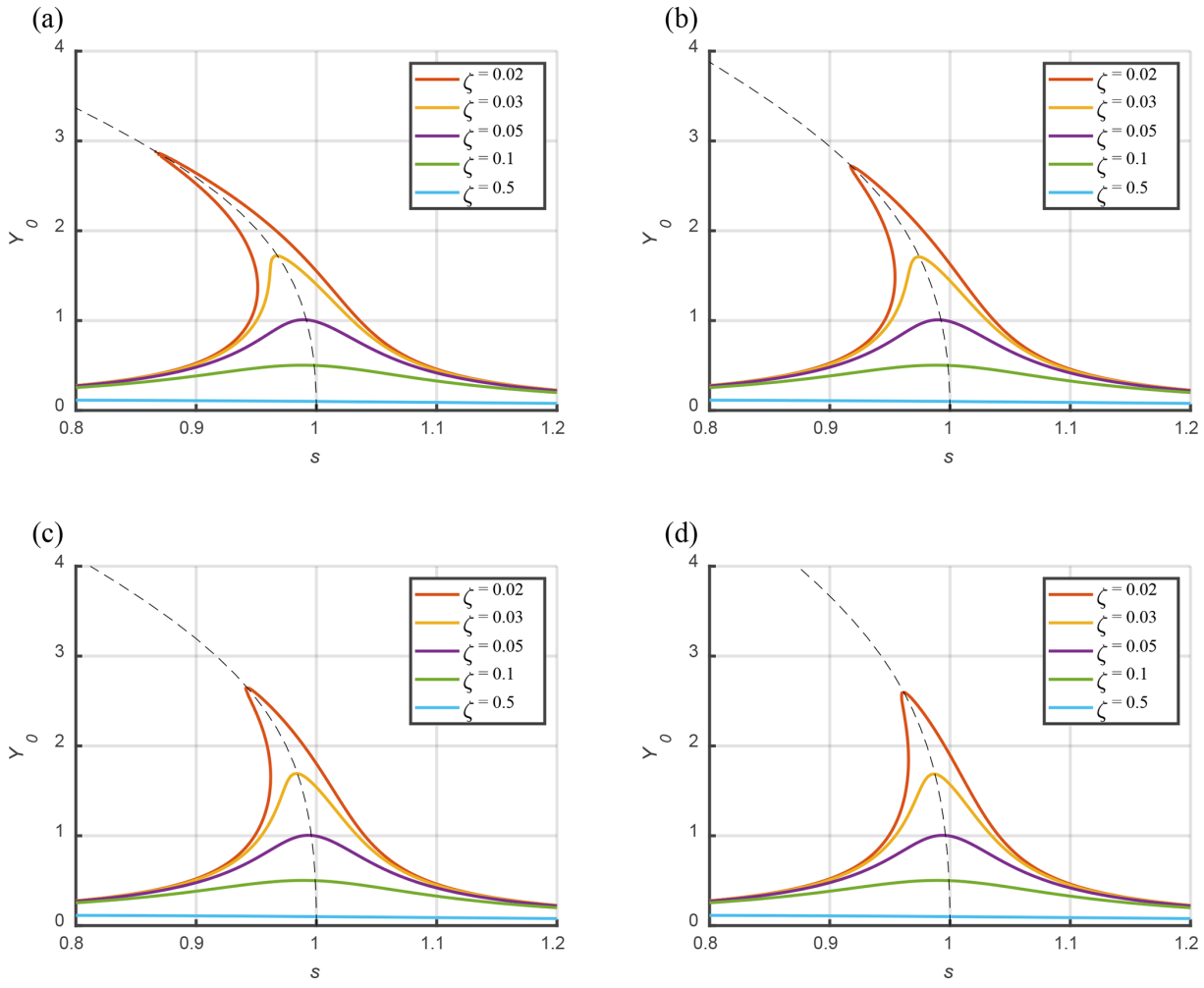

Figure 6. Amplitude–frequency characteristic and the backbone (represented by the dashed black line) of the blade-virtual-mass testing system: **(a)** $B = 0.1$, $\frac{3}{4}\varepsilon_2 = 0.01$, $\frac{10}{16}\varepsilon_4 = 0.002$; **(b)** $B = 0.1$, $\frac{3}{4}\varepsilon_2 = 0.01$, $\frac{10}{16}\varepsilon_4 = 0.001$; **(c)** $B = 0.1$, $\frac{3}{4}\varepsilon_2 = 0.005$, $\frac{10}{16}\varepsilon_4 = 0.001$; **(d)** $B = 0.1$, $\frac{3}{4}\varepsilon_2 = 0.005$, $\frac{10}{16}\varepsilon_4 = 0.0005$.

necessary to take further transient sweep-frequency analysis to obtain the resonance characteristics of the system.

3.1 Simulation modeling

To verify that the simplified equivalent theoretical model can reflect the characteristics of the actual test system, the simulation model is established in software. Generally, only the cross-section stiffness (flap-wise and edge-wise) and linear density are considered in the simulation model (Post and Bürkner, 2016) because the torsional natural frequency is much higher than the natural frequency in the flap-wise and edge-wise directions, and it is difficult to stimulate large torsional deformation. The root of the blade was set as a fixed constraint to simulate the cantilever beam condition similar to when the blade is mounted on the test rig. The equivalent damping ratio of the blade changes during vibration, resulting in a change in the resonance frequency of the test system (Lee and Lee, 2018; Liu et al., 2019). In order to accurately assess the influence of virtual masses on the characteristics of the testing system, aerodynamic damping is not considered in the simulation model. The blade model was built in the simulation software based on the parameters mentioned above, as shown in Fig. 7a.

3.2 Model validity verification

To ensure the applicability and rationality of the model, modal analysis is carried out and compared with the transfer matrix method (TMM) and the test data, as shown in Table 1. The transfer matrix method is an approximate theoretical method used to calculate the natural frequencies and modes of systems with chain structures. The transfer matrix method separates the structure with inertia and elasticity and obtains the relationship between the discrete elements. The natural frequencies and modes of the systems can be solved

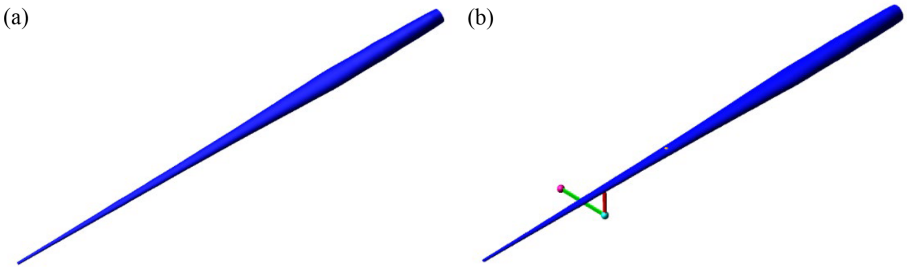

Figure 7. Dynamic simulation model of test system: **(a)** the blade simulation model and **(b)** the blade-virtual-mass simulation model (flap-wise).

Table 1. Comparison of natural frequencies calculated by various methods.

Flap-wise	84 m		94 m	
method	First modal frequency [Hz]	Error [%]	First modal frequency [Hz]	Error [%]
Test	0.394	–	0.365	–
TMM	0.397	+0.7	0.349	−4.38
simulation	0.404	+2.54	0.377	+3.29
Edge-wise	84 m		94 m	
method	First modal frequency [Hz]	Error [%]	First modal frequency [Hz]	Error [%]
Test	0.590	–	0.571	–
TMM	0.604	+2.37	0.561	−1.75
simulation	0.610	+3.34	0.589	+3.15

according to the boundary conditions. The transfer matrix method belongs to the physical discrete method of continuous systems, which is suitable for numerical solution of blade models. The blades in Table 1 were all subjected to actual modal tests, and the obtained frequency data are obtained from the frequency domain analysis of actual test data. The actual blade modal test was carried out by the hammer method. It can be seen that the simulation model of the test system has good applicability, with an error in the modal frequency of less than 4 %.

3.3 Simulation setup

With the purpose of demonstrating the nonlinear effects of rotating virtual masses on the testing system, it is necessary to add virtual masses based on the blade model, as shown in Fig. 7b. The values of the tuning masses are shown in Table 2, and the section properties of the blades are shown in Fig. 8. The position and values of the tuning masses are provided by the blade manufacturer. Virtual mass elements and exciting force are added at 62 % and 49 % of the 84 m blade length in the flap-wise and edge-wise directions respectively. Similarly, virtual mass elements and exciting force are added at 63 % and 52 % of the 94 m blade length in the flap-wise and edge-wise directions respectively (masses marked in bold in Table 2). The constraints for the seesaw, push rod and virtual masses are set according to Fig. 1, where the rotation center of the seesaw is set as the revolute pair, and the seesaw and push rod are set as the rigid light rod. To evaluate and verify the effects of virtual mass installation parameters and blade response on the vibration characteristics of the test system, not only the effects of the radius of the seesaw and blade response on the resonance frequency but also the effects of the radius of the seesaw on the load distribution of the blade with similar amplitude are analyzed through simulation.

4 Results

According to the backbone in the amplitude–frequency characteristic curve of the blade-virtual-mass test system, when the operation condition is determined, the square of the resonance frequency and the blade amplitude satisfy the relationship in Eq. (18). Thus, correlated simulation results are fitted using relevant functions to verify the relationship.

4.1 Effects of virtual masses on uniaxial test

4.1.1 Effects of blade amplitude on resonance frequency

Set $R = 4$ m and $L = 4$ m and investigate the variation in the resonance frequency of the test system at different amplitudes. Sweep-frequency analysis is performed on the 84 m and 94 m blades in the flap-wise and edge-wise directions respectively to obtain the resonance frequencies of the test system under different steady-state amplitudes, while the results are fitted according to Eq. (18), as shown in Fig. 9. In addition, the degree of fit is expressed by goodness of fit R^2. The sweep-frequency range is defined as a bandwidth of 0.02 Hz near the first natural frequency in the flap-wise or edge-wise direction, with an action time of 1×10^4 s and a resolution of 2×10^{-6} Hz s^{-1}. The frequency spectrum of the displacement of the exciting point of the blade under the sweeping

Table 2. Blade additional masses of 84 and 94 m blade. Bold values indicate the values and position of the virtual mass in the flap-wise or edge-wise directions.

84 m			94 m		
Location	Flap-wise masses [kg]	Edge-wise masses [kg]	Location masses [kg]	Flap-wise masses [kg]	Edge-wise
26 %		2835	42 %	3000	3000
36 %		3147	52 %		**4075**
49 %	6120	**4075**	63 %	**1116**	
62 %	**1117**				

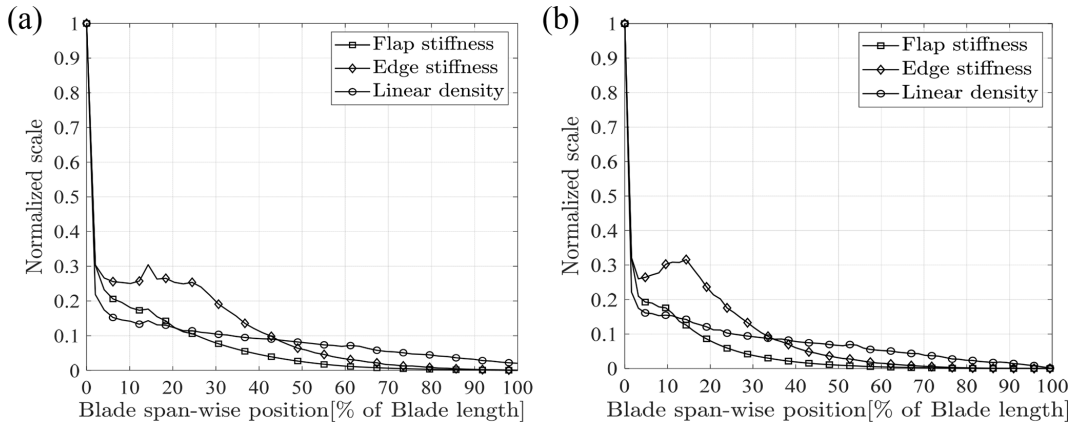

Figure 8. Section properties of the blade: **(a)** 84 m blade and **(b)** 94 m blade.

excitation is analyzed, and the frequency corresponding to the peak point is the resonance frequency. The mechanism might reach the geometric limit of the push rod parallel to the seesaw, so the limit requirements of the mechanism need to be considered.

When the amplitude of the blade is small, the percentage drop in resonance frequency is small. When the amplitude of the blade is large, the resonance frequency decreases nonlinearly faster. When the blade amplitude in the flap-wise direction reaches 2.6 m, the resonance frequency of the 84 and 94 m blades decreases by approximately 2.0 %; when the blade amplitude in the edge-wise direction reaches 2.2 m, the resonance frequency of the 84 and 94 m blades decreases by only approximately 1.1 %. Due to the limitation of resonance frequency extraction precision in sweep-frequency analysis, the fitting degree of data is affected. However, it is still acceptable at the large amplitude of the blade. Combined with the actual test requirements, we should pay more attention to the conditions of large amplitude.

Taking a 94 m blade as an example, the sweep spectrum of the blade under different target amplitudes is shown in Fig. 10. It can be seen from Fig. 10 that different excitation frequencies cause different blade responses. The resonance frequency of the system decreases with an increase in the maximum amplitude of the blade. This also verifies the applicability of the approximate amplitude–frequency properties obtained by the theory (Fig. 6 has a backbone curve similar to Fig. 10).

4.1.2 Effects of radius of the seesaw on resonance frequency and load distribution

Considering the actual test setup, the blade amplitude in the flap-wise direction is set to be about $Y = 2$ m, and the length of the push rod is $L = 4$ m; the blade amplitude in the edge-wise direction is about $Y = 1$ m, and the length of the push rod is $L = 4$ m. The sweep-frequency analysis of the 84 and 94 m blades in the flap-wise and edge-wise directions is carried out respectively to obtain the resonance frequency of the test system. According to Eq. (18), an appropriate function (Eq. 19) is selected to fit the results, as shown in Fig. 11. Equation (18) is a function selected according to the degree of best fit. Considering Eqs. (18) and (19), the small parameters encompass the influence of the radius of the seesaw, which can be approximated by an exponential function. A larger radius of the seesaw results in a smaller decrease in the resonance frequency. Conversely, when the rotation radius of the seesaw is small, the resonance frequency experiences a nonlinear decrease. With $R = 3$ m, the drop in the resonance frequency of the 84 and 94 m blades is approximately 1.6 %

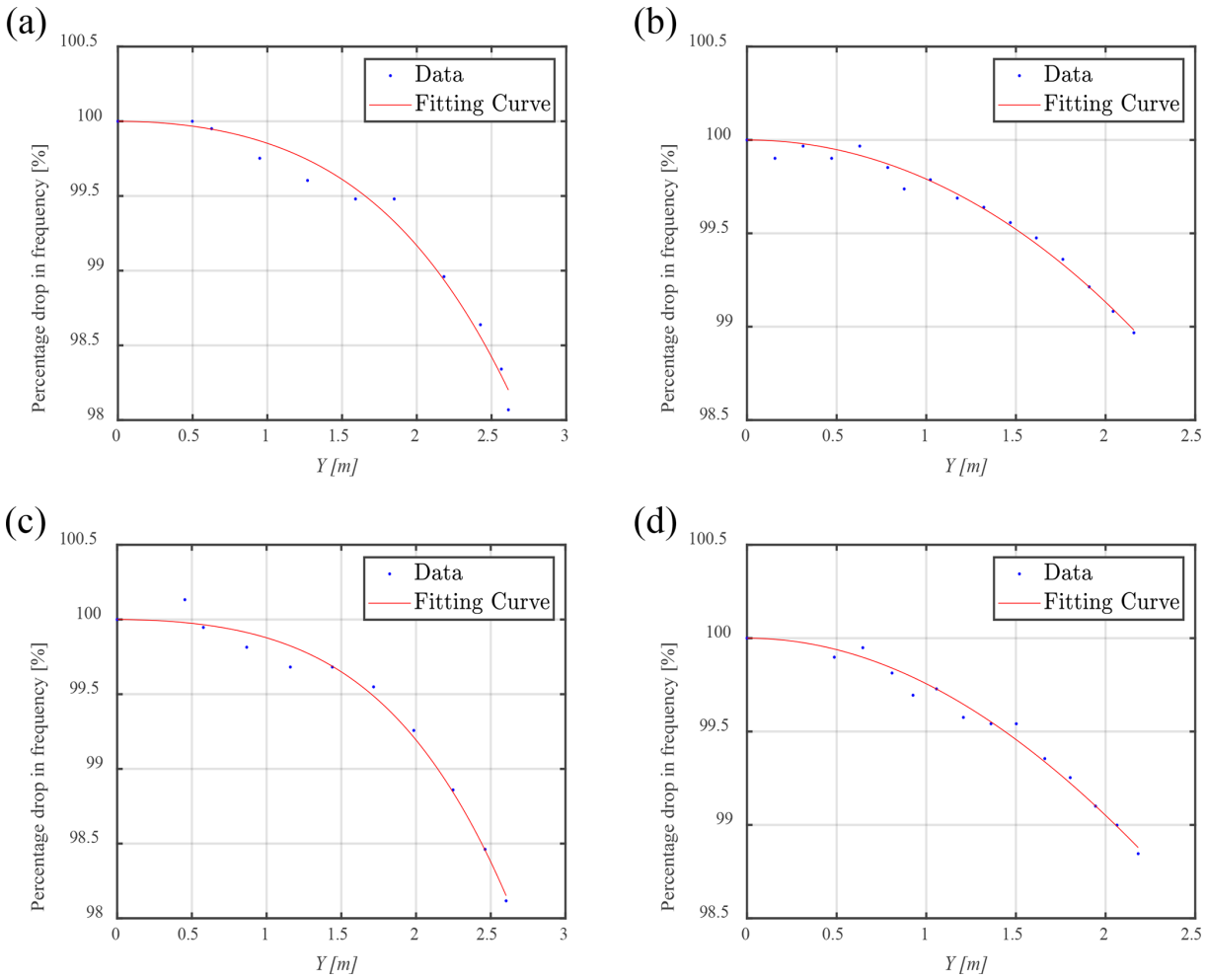

Figure 9. Relationship between amplitude and percentage drop in resonance frequency: **(a)** 84 m blade in the flap-wise direction ($R^2 = 0.9814$), **(b)** 84 m blade in the edge-wise direction ($R^2 = 0.9829$), **(c)** 94 m blade in the flap-wise direction ($R^2 = 0.9861$), **(d)** 94 m blade in the edge-wise direction ($R^2 = 0.9831$).

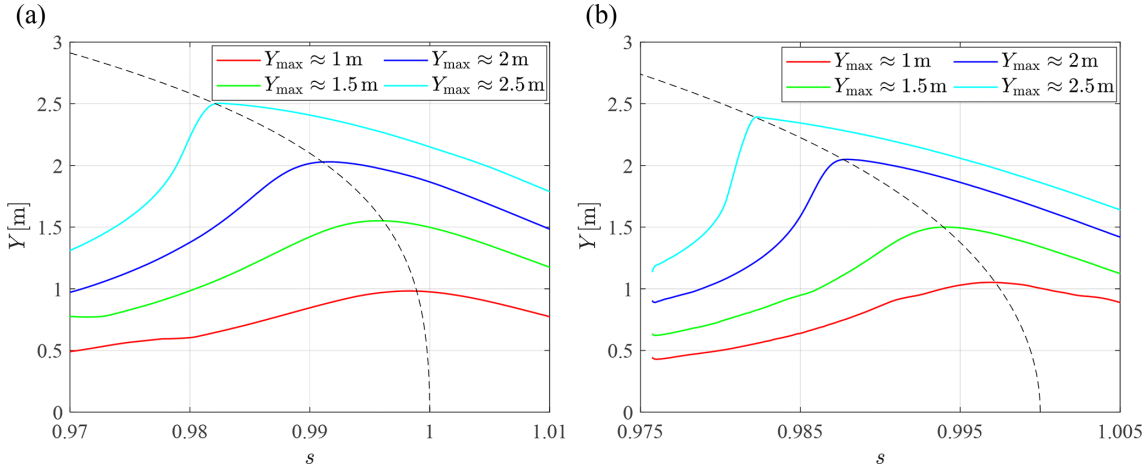

Figure 10. The sweep spectrum of the blade under different target amplitudes.

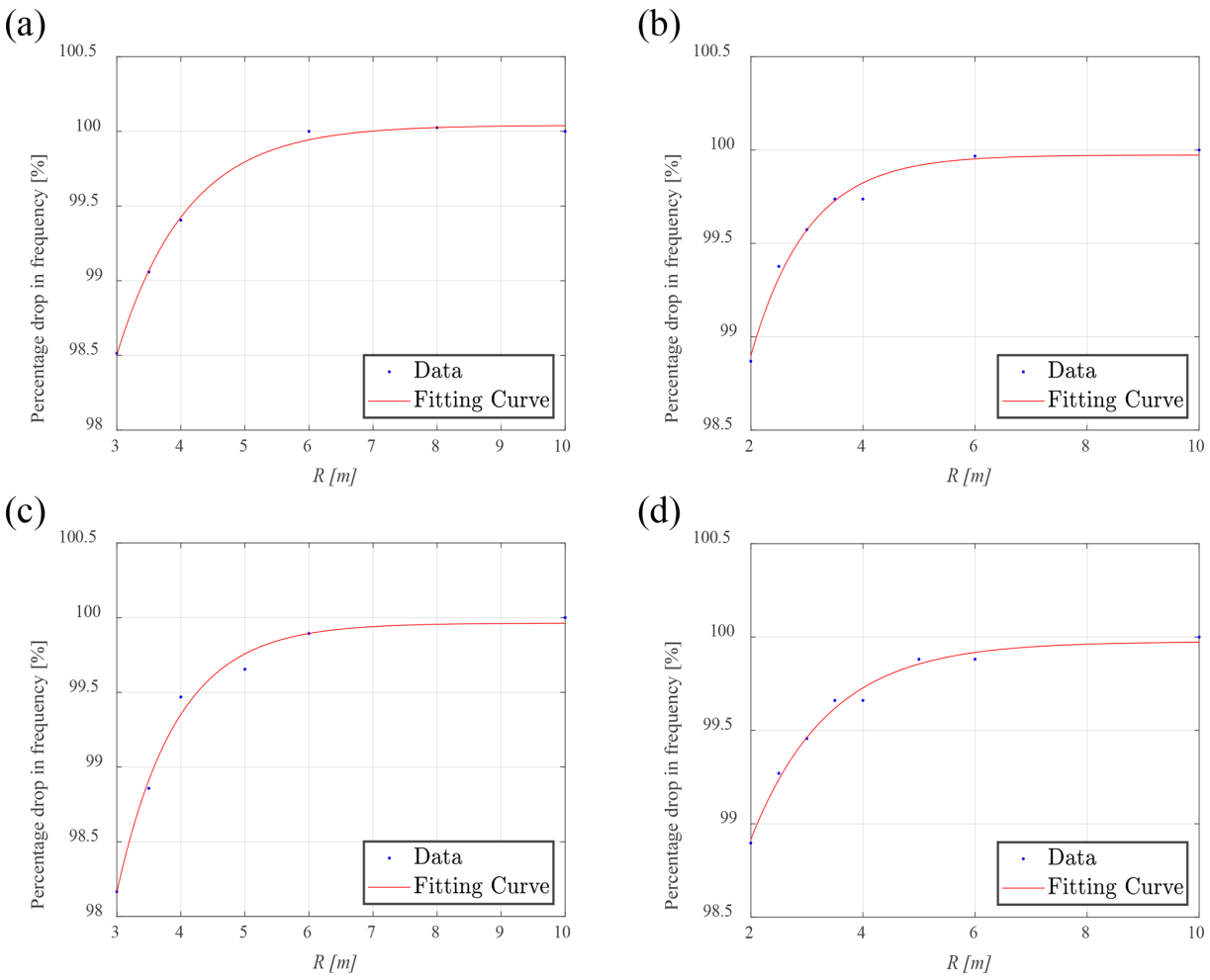

Figure 11. Relationship between radius of the seesaw and percentage drop in resonance frequency: **(a)** 84 m blade in the flap-wise direction ($R^2 = 0.9973$), **(b)** 84 m blade in the edge-wise direction ($R^2 = 0.9786$), **(c)** 94 m blade in the flap-wise direction ($R^2 = 0.9884$), **(d)** 94 m blade in the edge-wise direction ($R^2 = 0.9890$).

in the flap-wise direction. Likewise, with $R = 2$ m, the drop in the resonance frequency is only approximately 1.1 % in the edge-wise direction.

$$\omega^2 = \frac{\omega_n^2}{\left(1 + ae^{-bR}\right)}, \tag{19}$$

where a and b are parameters in exponential function.

In order to compare the influence of nonlinearity on the blade load distribution, the blade bending moment distribution can be calculated by using constant displacement of the exciting point and inertial load provided by virtual mass motion. The excitation position is the same as the installation position of the virtual masses closest to the tip of the blade, and the specific values are shown in Table 2. The excitation frequency is the resonance frequency of the respective vibration direction, which is obtained by the sweep-frequency analysis.

The radius of the seesaw influences the characteristics of the testing system and alters the distribution of blade loads, as shown in Fig. 12. In the case of $R = \infty$, the virtual masses shift from rotation to translation in the uniaxial test, effectively simulating additional masses that are directly fixed onto the blade. Consequently, there is an approximate 3 % decrease in the overall load distribution in the flap-wise direction; the area which is actually fully tested will be reduced. Given the roughly similar amplitudes, lower resonance frequency results in reduced inertial loads on the blade. Therefore, compensatory measures such as increasing the excitation level are necessary during the actual test. However, this requires more powerful excitation equipment.

4.2 Effects of virtual masses on biaxial test

In Sect. 4.1, only the effect of virtual masses on the uniaxial test is considered, which can intuitively indicate the influence of independent parameters on the vibration characteristics of

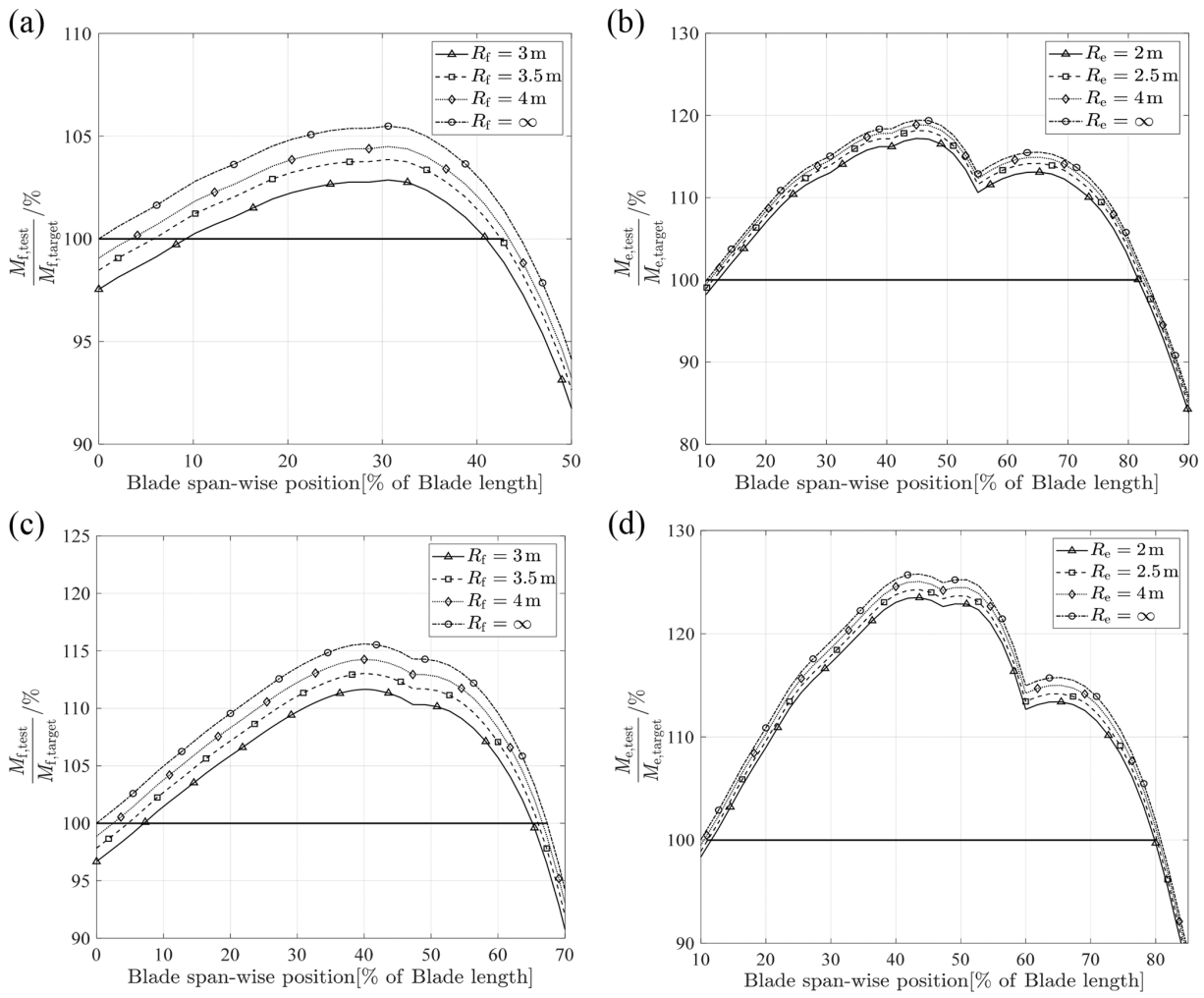

Figure 12. Relationship between radius of the seesaw and blade load distribution: **(a)** 84 m blade in the flap-wise direction, **(b)** 84 m blade in the edge-wise direction, **(c)** 94 m blade in the flap-wise direction and **(d)** 94 m blade in the edge-wise direction.

the test system and blade load distribution from the uniaxial model. However, it is not enough to consider only the uniaxial vibration, but also the effect of virtual masses on the system in the biaxial vibration. In the biaxial test, the blade has a complex spatial trajectory, and the test system will be affected by multiple nonlinear parameters at the same time. To find the resonance frequency of the two directions, it is necessary to use the simulation software for iterative calculation.

Taking a 94 m blade as an example, virtual masses are applied in both the flap-wise and edge-wise directions. Modal analysis and sweep-frequency analysis are used to obtain the frequencies at which specific excitations are applied to the test system. Combined with the actual working conditions, the flap amplitude at the 63 % position of the blade is about 2 m, and the edge amplitude at the 52 % position of the blade is about 1 m. The resonance frequencies under different conditions are shown in Table 3, with $R = 4$ m and $L = 4$ m. In fact, the oscillations in the flap-wise and edge-wise direction must not be evaluated separately as they influence each other, so the resonance frequency of the blade in each direction is obtained by sweeping frequency iteration. Figure 13 shows the spatial trajectory of the blade under the action of different virtual mass mechanisms. The results show three main characteristics. (1) Under the same exciting force, the resonance frequency of the two directions in the biaxial test is lower than that of the uniaxial test, which indicates that the virtual masses affect both vibration directions. (2) Compared with the ideal working condition, the virtual masses will deform the space trajectory of the blade (even considering the structural torsion of the blade), which is determined by the motion characteristics of the mechanism. In addition, the deformation of the trajectory may bring higher requirements for the actual damage assessment of the blade. (3) Under the same exciting force, the difference between the average flap amplitude of the blade using the rotating-virtual-mass mechanism

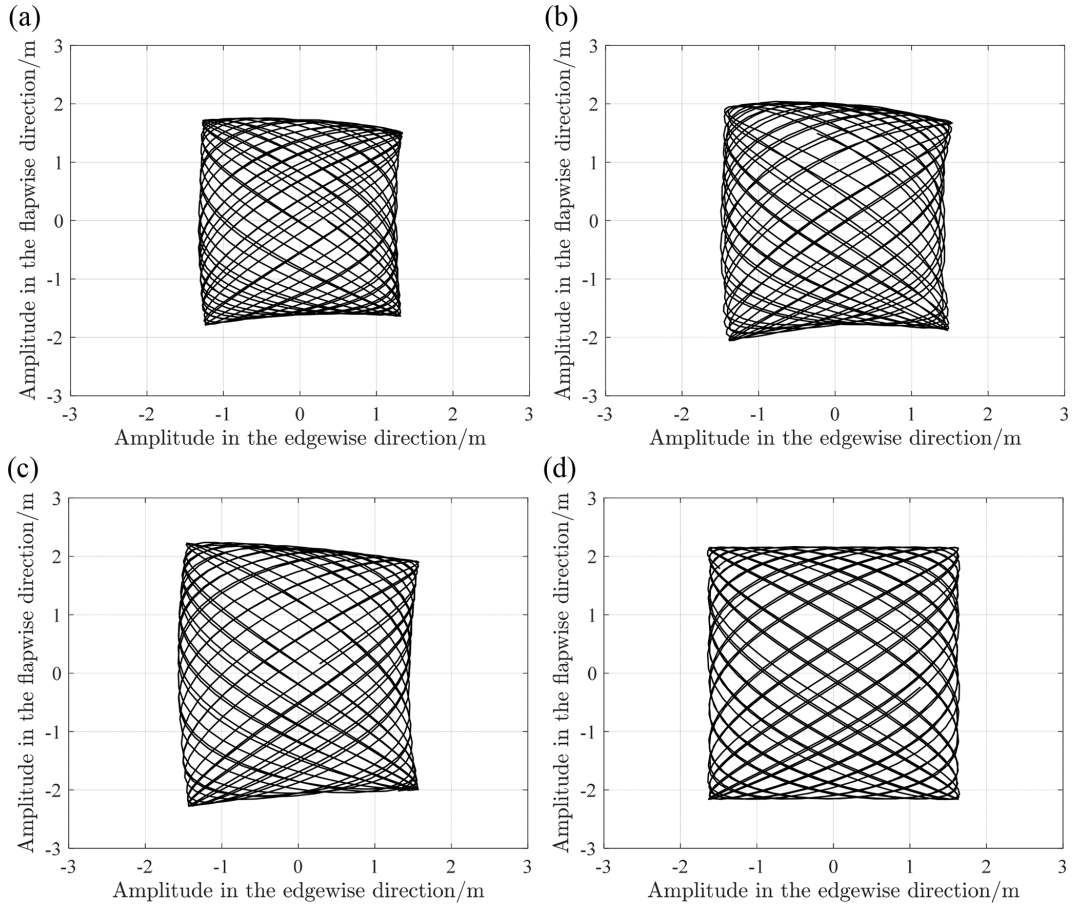

Figure 13. Biaxial trajectory of blade-virtual-mass test system with the same exciting force (at 63 % of the blade position): **(a)** natural frequency excitation, **(b)** resonance frequency excitation (rotation), **(c)** resonance frequency excitation (actual translation), **(d)** resonance frequency excitation (ideal translation).

Table 3. Biaxial excitation parameters of 94 m.

	Virtual masses and exciting point		Natural frequency	Sweep-frequency analysis			
				Uniaxial	Biaxial resonance frequency [Hz]		
	Position [%]	Force [N]	[Hz]	resonance frequency (rotation) [Hz]	Rotation	Actual translation	Ideal translation
Flap	63 %	3800	0.377	0.373	0.369	0.375	0.377
Edge	52 %	7000	0.589	0.587	0.583	0.587	0.589

and the average flap amplitude under the ideal condition is 9 %, and the difference between the average edge amplitude and the average edge amplitude under the ideal condition is nearly 11 %, as shown in Table 4. Combined with the effect of reduced resonance frequency and amplitude, the biaxial load distribution level of the blade will be further reduced compared with the uniaxial test, which means that more energy input is required.

5 Conclusion

The nonlinear effect of the virtual mass device on the blade test system is discussed in this paper. Under actual working conditions, the test system is limited by the size of the virtual mass mechanism and the amplitude of the blade, and its resonance characteristics will be changed. This paper analyzes the nonlinearity of the system resonance characteris-

Table 4. Biaxial amplitude of 94 m.

	Biaxial average amplitude [m]		
	Rotation	Actual translation	Ideal translation
Flap	1.923	2.113	2.154
Edge	1.447	1.511	1.630

tics from the mechanism of the change in the inertia force of the virtual mass and establishes a blade uniaxial theoretical model to explore the influence of the amplitude of the blade and the size of the seesaw on the resonance frequency. Based on the above content, the approximate nonlinear amplitude–frequency characteristic curve of the test system is obtained. Then the software is used to simulate the two blades by the transient sweep method, and the applicability of the theoretical model is verified.

For the uniaxial theoretical model, the increase in blade amplitude, the shortening of seesaw size and the increase in counterweight mass will reduce the resonance frequency in the main vibration direction. However, the uniaxial simulation results of two blades show that the amplitude of the blade or the size of the seesaw have limited influence on the resonance frequency. For example, when the size of the mechanism is unchanged ($L = R = 4$ m), only the influence of the blade amplitude on the system is considered. When the amplitude of the flapping direction increases to 2.6 m, the resonance frequency in this direction decreases by nearly 2 % compared with the natural frequency. Combined with the actual working conditions, when the amplitude of the flap-wise direction is maintained at about 2 m, the length of the seesaw is shortened to 3 m, and the resonance frequency is reduced by nearly 2 %. The target amplitude of the edge-wise direction is usually small compared with the flap-wise direction, so shortening the length of the seesaw only reduces the resonance frequency by 1.1 %. In the case of the same amplitude, the shortening of the seesaw length will reduce the blade load distribution level, and the flap-wise load level will decrease by up to 3 % at most. Due to the small amplitude of the edge-wise direction, the load level in this direction does not drop significantly.

Although the nonlinear factors have less influence on the uniaxial test, they have more influence on the biaxial test. Under the same excitation force and approximate target amplitude ($Y \approx 2$ m), the rotating virtual masses induce lower resonance frequency in biaxial vibration than in uniaxial tests (flap-wise direction: 1.06 % decrease in uniaxial vibration, 2.12 % decrease in biaxial vibration; edge-wise direction: 0.34 % decrease in uniaxial vibration, 1.02 % decrease in biaxial vibration). In addition, under the same exciting force, the difference between the average flap amplitude of the blade using the rotating-virtual-mass mechanism and the average flap amplitude under the ideal condition is 9 %, and the difference between the average edge amplitude and the average edge amplitude under the ideal condition is nearly 11 %. Furthermore, the virtual mass mechanism can also cause the deformation of the space trajectory envelope of the blade. Under the combined action of many factors, the nonlinear effect will be further strengthened.

In conclusion, the virtual mass mechanism will bring a nonlinear effect to the test system due to its own motion characteristics, and the nonlinear factors mainly include the amplitude of the blade, the size of the mechanism and the mass of the counterweight. In the case of small amplitude, the nonlinear effect is not obvious and does not have a great influence on the blade load level. In the biaxial large-amplitude test, the nonlinear effect is enhanced, and the blade trajectory is deformed. The resonance frequency of the system will be further reduced. Under the same excitation, the actual blade amplitude is less than the target amplitude. These characteristics mean that the biaxial test requires larger excitation equipment and higher requirements for blade damage calculation and load formulation.

Code and data availability. The data that support the findings of this research are not publicly available due to confidentiality constraints.

Author contributions. JS conceptualized and defined the requirements for the method developed. AZ supervised the work. JS and TD developed the model code and performed the simulations. JS prepared the manuscript with contributions from all coauthors.

Competing interests. The contact author has declared that none of the authors has any competing interests.

Disclaimer. Publisher's note: Copernicus Publications remains neutral with regard to jurisdictional claims made in the text, published maps, institutional affiliations, or any other geographical representation in this paper. While Copernicus Publications makes every effort to include appropriate place names, the final responsibility lies with the authors.

Acknowledgements. We appreciate that Aeolon Technology Co., Ltd provided the personnel assistance and technical support.

Financial support. Blade data of this research have been supported by Aeolon Technology Co., Ltd.

Review statement. This paper was edited by Weifei Hu and reviewed by David Melcher, Qingshan Yang, and one anonymous referee.

References

Castro, O., Belloni, F., and Stolpe, M.: Optimized method for multiaxial fatigue testing of wind turbine blades, Compos. Struct., 257, 113358, https://doi.org/10.1016/j.compstruct.2020.113358, 2021.

DNV GL AS: DNVGL-ST-0376 – Rotor blades for wind turbines, https://rules.dnvgl.com/docs/pdf/DNVGL/ST/2015-12/DNVGL-ST-0376.pdf (last access: 7 June 2019), 2015.

Falko, B.: Biaxial Dynamic Fatigue Tests of Wind Turbine Blades, PhD thesis, Leibniz University Hannover, Hannover, Germany, https://publica.fraunhofer.de/handle/publica/283519 (last access: 28 October 2023), 2020.

Greaves, P. R., Dominy, R. G., Ingram, G. L., Long, H., and Court, R.: Evaluation of dual-axis fatigue testing of large wind turbine blades, P. I. Mech. Eng. C-J. Mec., 226, 1693–1704, https://doi.org/10.1177/0954406211428013, 2012.

Hughes, S., Musial, W. D., and Stensland, T.: Implementation of a Two-Axis Servo-Hydraulic System for Full-Scale Fatigue Testing of Wind Turbine Blades, Tech. rep., National Renewable Energy Lab., Golden, CO, USA, https://www.osti.gov/servlets/purl/12200 (last access: 28 October 2023), 1999.

IEC: IEC 61400-23 – Wind Turbines Part 23: Full-scale Structural Testing of Rotor Blades, IEC, Geneva, Switzerland, 2014.

Lee, H. G. and Lee, J.: Damping mechanism model for fatigue testing of a full-scale composite wind turbine blade, Part 1: Modeling, Compos. Struct., 202, 1216–1228, https://doi.org/10.1016/j.compstruct.2018.05.124, 2018.

Liao, G. H. and Wu, J. Z.: Vibration Analysis of a Dual-axial Fatigue Loading System for Wind Turbine's Blades Test, Noise Vibrat. Control, 34, 114–116, https://doi.org/10.3969/j.issn.1006-1335.2014.05.026, 2014.

Liao, G. H. and Wu, J. Z.: Wind turbine blade resonance fatigue loading system and experiment, Acta Energ. Sol. Sin., 37, 2785–2791, 2016.

Liu, Y. Z. and Chen, L. Q.: Nonlinear vibrations, Higher Education Press, https://www.dushu.com/book/10052149/ (last access: 28 October 2023),, 2001.

Liu, Y. Z., Chen, L. Q., and Chen, W. L.: Mechanics of Vibration, Higher Education Press, https://xuanshu.hep.com.cn/front/book/findBookDetails?bookId=5bed82d7f18f967ee7f37a8a (last access: 28 October 2023), 2019.

Lu, L., Zhu, M., and Wu, H.: A Review and Case Analysis on Biaxial Synchronous Loading Technology and Fast Moment-Matching Methods for Fatigue Tests of Wind Turbine Blades, Energies, 15, 4881, https://doi.org/10.3390/en15134881, 2022.

Melcher, D., Bätge, M., and Neßlinger, S.: A novel rotor blade fatigue test setup with elliptical biaxial resonant excitation, Wind Energ. Sci., 5, 675–684, https://doi.org/10.5194/wes-5-675-2020, 2020a.

Melcher, D., Petersen, E., and Neßlinger, S.: Off-axis loading in rotor blade fatigue tests with elliptical biaxial resonant excitation, J. Phys.: Conf. Ser., 1618, 052010, https://doi.org/10.1088/1742-6596/1618/5/052010, 2020b.

Melcher, D., Rosemann, H., and Haller, B.: Proof of concept: elliptical biaxial rotor blade fatigue test with resonant excitation, IOP Conf. Ser.: Mat. Sci. Eng., 942, 012007, https://doi.org/10.1088/1757-899X/942/1/012007, 2020c.

Post, N. and Bürkner, F.: Fatigue Test Design: Scenarios for Biaxial Fatigue Testing of a 60-Meter Wind Turbine Blade, Tech. rep., National Renewable Energy Lab., Golden, CO, USA, https://doi.org/10.2172/1271941, 2016.

Snowberg, D., Dana, S., Hughes, S., and Berling, P.: Implementation of a Biaxial Resonant Fatigue Test Method on a Large Wind Turbine Blade, Tech. rep., National Renewable Energy Lab., Golden, CO, USA, https://doi.org/10.2172/1155105, 2014.

White, D.: New method for dual-axis fatigue testing of large wind turbine blades using resonance excitation and spectral loading, Tech. rep., National Renewable Energy Lab., Golden, CO, USA, https://doi.org/10.2172/15007390, 2004.

Zhang, J. B., Shi, K. Z., and Zhang, C. Y.: Improving accuracy of dual-axial resonance fatigue testing for wind turbine blades by using predicted equivalent test loads caused by combined loading, J. Renew. Sustain. Energ., 12, 013303, https://doi.org/10.1063/1.5112006, 2020.

Zhang, L. A. and Huang, X. M.: Study of wind turbine blade vibration characteristics under single point fatigue load driven, Acta Energ. Sol. Sin., 36, 1112–1116, https://doi.org/10.3969/j.issn.0254-0096.2015.05.013, 2015.